Quantum random walk search optimization using resetting techniques

Hugo Jongeneelen

Faculty of Electrical Engineering, Mathematics and Computer Science

Delft University of Technology

Supervisors

Dr. Johan Dubbeldam

Prof. Dr. Yaroslav Blanter

In partial fulfillment of the requirements for the degrees of

BSc Applied Mathematics

BSc Applied Physics

December 18, 2024

Abstract

Quantum algorithms have shown much potential in solving complex problems more efficiently than our current classical algorithms, particularly in search problems with a large and complex search space. When leveraging the principles of superposition and interference, quantum walk based algorithms can lead to a faster convergence on a target state.

The thesis begins with a theoretical framework for the study of classical and quantum walks on graphs. The usage in search algorithms is discussed together with the effect of a modified Hamiltonian that introduces a bias toward the target state. This is analyzed using perturbation theory showing a decrease of the ground state energy.

Ultimately, this thesis focuses on the optimization of quantum random walk search algorithms using resetting techniques. Simulations of quantum random walks on simple graph structures, such as path and cycle graphs are used to provide concrete examples. Results show that resetting not only improves the probability of finding the target state, but also has a faster convergence. Furthermore, decoherence effects are shown to be reduced when using resetting techniques.

Contents

Chapter 1

Introduction

In recent years, quantum mechanics and quantum computing have received more and more attention. This is driven by the potential for a revolutionary development in the complexity of computations and more efficient algorithms. Traditional algorithms often end up with problems that have an exponential growth in computational time, especially in search problems where the search space can be very complex. On the other hand, quantum algorithms, which can be based on quantum walks, have interesting properties like superposition that can improve the search efficiency [1].

In this thesis, we will take an extensive look at how we can optimize quantum random walk search by using resetting techniques. These quantum random walks are essential for various quantum algorithms, having unique advantages over their classical counterpart. For example, properties like interference and the ability to go on multiple paths simultaneously lead to a faster convergence on target states in a search process. However, in practical applications, there are many challenges due to decoherence, which limits the efficiency of quantum algorithms. By using resetting techniques, you can reset the walker to specific states or a superposition of states such that the decoherence is countered and the search process can be optimized.

Before we get there however, we first discuss the foundational concepts in quantum mechanics, graph theory, and random walks which are needed to under-

stand the quantum systems that will come later. This theoretical framework in Chapter 2 begins with a review of quantum mechanics, specifically the role of density matrices and the Lindblad master equation for describing evolution in open quantum systems. In contrast with the Schrödinger equation, which is applied to closed quantum systems, the Lindblad equation accounts for interaction with the environment, causing decoherence. This makes it an important tool to study real-world quantum systems.

We then discuss graph theory as a framework for representing the search space and introduce the classical and quantum random walk. The graph will serve as the mathematical structure that determine the movement of the walker. A modified Hamiltonian is used for the quantum random walk to introduce a bias toward the target state. This will be analyzed using perturbation theory, which gives more insight into the energy landscape and how the bias affects this landscape.

Simulations of the quantum random walks in Chapter 3 are conducted on various graphs to provide concrete examples of how the walker traverses the graph. These graphs have different topologies which influence the quantum walk. The modified Hamiltonian that introduces a bias and convergence to the target state is also demonstrated.

In the final section, Chapter 4, we introduce two resetting techniques as a method to optimize the quantum random walk search. This involves resetting the walker to a predefined superposition of states. By doing so, decoherence effects are reduced and the search efficiency is improved. One approach to resetting is a constant resetting rate towards a fixed dimensionality reset state. This reset state is a superposition and will be dynamic to increase the search efficiency. The second approach uses a variable dimensionality reset state that converges to the pure target state. The simulations show that these techniques can be used to optimize the probability of finding the target state, while minimizing the time that it takes.

Chapter 2

Theory

2.1 Quantum mechanics

In this section, we will present a short overview of the formalism from quantum mechanics that is used to formulate the quantum random walk.

2.1.1 Density matrices

When dealing with quantum states, we never know the exact state of a system unless we measure it. To still be able to work with this, we introduce density matrices as a way of describing mixed states, where the system is in a probabilistic combination of multiple *pure* states which are denoted by $|\Psi_k\rangle \in \mathcal{H}$, where $\mathcal{H}$ is the Hilbert space of the system. Suppose for instance that the probability of being in state $|\Psi_k\rangle$ is p_k, then the density matrix is defined in the following way:

$$\rho \equiv \sum_k p_k \left|\Psi_k\right\rangle \left\langle\Psi_k\right|,$$

where $\langle\Psi_k|$ is the Hermitian conjugate of $|\Psi_k\rangle$.

This density matrix ρ possesses several important properties:

- **Hermitian**: The density matrix is Hermitian because it is constructed of Hermitian outer products $|\Psi_k\rangle \langle\Psi_k|$. Therefore, we also have that $\rho^\dagger = \rho$ and is thus Hermitian.

- **Positive Semi-Definite**: For any vector $|\phi\rangle \in \mathcal{H}$, the probability of obtaining the measurement outcome $|\phi\rangle$ is given by the expecation value $\langle\phi|\,\rho\,|\phi\rangle$, which is always non-negative. This non-negativity results from the fact that each term in the sum defining ρ is positive semi-definite. Specifically, $p_k \geq 0$ and $|\Psi_k\rangle\langle\Psi_k|$ is positive semi-definite for any $|\Psi_k\rangle$.
- **Trace Equals One**: The trace of the density matrix is one, $\mathrm{Tr}(\rho) = 1$, which reflects the property that the total probability of all possible pure states is normalized.

The diagonal elements of the density matrix $\hat{\rho}$ correspond to the probabilities of observing the system in each of the pure states $|\Psi_k\rangle$ [2]. The off-diagonal elements of the density matrix, on the other hand, represent the coherences between different pure states. Coherence in this case is the ability to be in a superposition of states, where the relative phases between the states are crucial.

2.1.2 Lindblad master equation

Although the motion of particles at the quantum level is described by the Schrödinger equation, we will be using the Lindblad master equation. The key distinction here is that the Schrödinger equation applies to closed systems, which is an idealised scenario of the real-world. To account for the interactions between particles and their surroundings, as is common in quantum computation, we will use the Lindblad master equation instead.

The Lindblad master equation can be derived from the von Neumann equation which is equivalent to the Schrödinger equation when applied to the density matrix framework [3]. The von Neumann equation describes the time evolution of the density matrix for a closed quantum system and is given by:

$$\frac{d\rho}{dt} = -i\,[H_Q, \rho]\,. \tag{2.1}$$

Here, the units are taken such that the reduced Planck's constant $\hbar = 1$ (this convention will be used throughout the thesis). The Hamiltonian H_Q is an operator that controls the dynamics of the quantum system. We will later show how this

Hamiltonian H_Q is constructed (see Equation (2.15)). When the Hamiltonian H_Q is time-independent, the solution to the von-Neumann equation is given by:

$$\rho(t) = U(t)\rho(0)U^\dagger(t) \tag{2.2}$$

with $U(t) = e^{-iH_Q t}$ being the unitary time-evolution operator and the dagger indicating the conjugate transpose. This however represents the idealised scenario of a closed system, where we assumed that there is no interaction with the environment and coherence is preserved. This quantum coherence refers to the property of a quantum system that is in a superposition of states and has specific phase relationships between them. As mentioned before, open quantum systems are on the contrary subject to interactions with their surrounding environment, distorting the phase relationships and causing decoherence [3]. The Lindblad equation (see Equation (2.3)) accounts for such effects by incorpating terms that model the dissipative effects of the environment. These effects, described by 'jump' operators L_{nm} can arise from various sources, such as interactions with the surrounding particles, electromagnetics fields and thermal fluctuations. The Lindblad master equation is denoted by:

$$\frac{d\rho}{dt} = -i[H_Q, \rho] + \sum_{nm} \left(L_{nm}\rho L_{nm}^\dagger - \frac{1}{2}\left\{L_{nm}^\dagger L_{nm}, \rho\right\} \right) \equiv \mathcal{L}\rho \tag{2.3}$$

with jump operators L_{nm} describing the jumps from $|n\rangle$ to $|m\rangle$. For example, L_{nm} could model the absorption and emission of a photon, where the system transitions from state $|n\rangle$ to $|m\rangle$. Furthermore, the notation of anticommutator $\{a, b\} = ab + ba$ is used and we have also defined the super-operator $\mathcal{L}$ such that it can be written as a first order differential equation.

As it turns out, we can implement different levels of coherence or dissipative effects from the environment by transforming Equation (2.3). This is also more realistic since a fully coherent walk is impossible to obtain in the real-world where you have to deal with varying levels of decoherence. To interpolate between a fully coherent (no influence from dissipative effects) and a fully incoherent evolution (random state transitions), we must introduce a dimensionless parameter $\epsilon \in \mathbb{R}_{\geq 0}$

such that we obtain the following equation [4]:

$$\frac{d\rho}{dt} = -i\left[(1-\epsilon)H_Q, \rho\right] - \epsilon \sum_{nm} \gamma_{nm} \left[\rho_{mm} \left|n\right\rangle \left\langle n\right| - \frac{1}{2}\{\left|m\right\rangle \left\langle m\right|, \rho\}\right]. \tag{2.4}$$

Here, ϵ represents the degree of quantum coherence. When $\epsilon \to 0$, it represents a fully coherent quantum walk which will be discussed in Subsection 2.3.2. Conversely, when $\epsilon \to 1$, it represents a fully incoherent walk, which is equivalent to a classical walk. To accurately represent the physical processes and interactions in the system, we have to define a set E to specify the pairs of states between which transitions can occur due to damping and decoherence. The jump operators, which represent these transitions can then be defined as $L_{nm} = \sqrt{\epsilon\gamma_{nm}} \left|n\right\rangle \left\langle m\right|$ for $(n, m) \in E$ with damping constants γ_{nm}. We will later see that we can write these jump operators using the classical Hamiltonian that is given in Subsection 2.3.1. For convenience, we express Equation (2.4) using the superoperator:

$$\frac{d\rho}{dt} = \mathcal{L}^{(\epsilon)}(\rho). \tag{2.5}$$

This is simulated in Section 3.1 for various levels of decoherence or dissipative effects that occur from an open system.

2.2 Networks

In the realm of networks, we are dealing with much more than just interconnected objects. Consider for instance a database network, where navigating through various data structures resembles the traversing of a complex network. In many of such cases, one aims to find specific information/files in the network, often seeking algorithms to aid in the task. This concept isn't limited to databases alone; various real-world situations, such as social networks, recommendation systems and biological systems, can be simplified and analysed using network principles. In this section, we will provide a framework for understanding such networks.

2.2.1 Graph theory

A network can be mathematically represented using a graph $G = (V, E)$, which consists of a set of vertices/nodes V (with $|V| = N \in \mathbb{N}$) and a set of edges $E \subseteq V \times V$ between the nodes. Characteristic properties of various graphs can be captured in two $n \times n$-matrices, the adjacency matrix A and the degree matrix D. The adjacency matrix describes which nodes are connected by an edge and has the following entries:

$$A_{ij} = \begin{cases} 1 & \text{if there is an edge from node } i \text{ to node } j, \\ 0 & \text{otherwise.} \end{cases}$$

In this thesis, we will only consider undirected networks, meaning that all edges are bidirectional between their associated nodes. This means that the adjacency matrix A is symmetric, as for any edge $(i, j) \in E$ present in the network, its reciprocal $(j, i) \in E$ also exists. Furthermore, no self-loops are allowed and there is only one edge allowed between any pair of nodes, making it a simple graph.

The diagonal degree matrix D denotes the degree k_i of each node. This is the number of edges connected to a certain node i and can be mathematically formulated as the sum over the i-th row in the adjacency matrix, i.e. $k_i = \sum_j^N A_{ij}$.

$$D_{ij} = \begin{cases} k_i & \text{if } i = j, \\ 0 & \text{otherwise.} \end{cases}$$

Both matrices are combined in the so-called Laplacian matrix, which will be used to formulate the classical random walk (CRW) and the quantum walk (QW) in Section 2.1. The symmetric Laplacian matrix $\mathfrak{L}$ (which should not be confused with the operator $\mathcal{L}$ defined in Equation (2.5)) is defined by:

$$\mathfrak{L} \equiv D - A, \qquad \text{with} \qquad \mathfrak{L}_{ij} = \begin{cases} k_i & \text{if } i = j \\ -1 & \text{if } (i, j) \in E \\ 0 & \text{otherwise} \end{cases} \tag{2.6}$$

2.3 Random walks

Random walks are a fundamental concept that is used in various fields, such as probability theory and statistical mechanics, describing the stochastic motion of particles or in our context, a walker. Applications of this concept include the so-called PageRank algorithm, which navigates through web pages to assess their relevance and rank them accordingly [5]. Furthermore, random walks are utilized to develop search algorithms and to characterize fluctuations on the stock market [6], [7]. The quantum counterpart has also demonstrated utility and, notably, surpasses its classical counterpart in certain scenarios, such as search algorithms [8]. In this section, we will outline both the classical random walk and its quantum counterpart.

2.3.1 Classical random walks (CRW)

A classical random walk represents the trajectory that is created by taking successive random steps on a given graph G. Beginning from an initial position or node, each step involves choosing one of the adjacent nodes. If a node has k adjacent nodes, then the probability of transitioning to any one of the adjacent nodes is $\frac{1}{k}$.

Consider a classical random walk on a graph as a continuous-time process. Define $p_i(t)$ to be the probability to be on node i at time t which can be represented in a probability vector:

$$\mathbf{p}(t) = (p_1(t), ..., p_N(t)) \qquad \text{with} \qquad \sum_{i=1}^{N} p_i(t) = 1 \quad \forall t$$

If the walker is on an arbitrary node j at time t, then we have that the probability to transition from node j to an adjacent node i is given by:

$$p_{j\to i} = \sum_{j=1}^{N} \frac{A_{ij}}{k_j} p_j(t) \tag{2.7}$$

Here, A_{ij} denotes the adjacency matrix element, and k_j is the degree of node j. The adjacency matrix ensures that only adjacent nodes from node i contribute to

the sum. The term k_j takes into account the degree of the node such that the walker does not necessarily have to go to i, but can go to other adjacent nodes with equal probability.

Now, if we consider a small time interval $[t, t + \Delta t]$ with Δt sufficiently small, the time evolution of the probability $p_i(t)$ can be described by calculating the probability of *going* to node i and subtracting the probability of *leaving* node i. This results in the following equation:

$$\begin{aligned} p_i(t + \Delta t) - p_i(t) &= \Delta t p_{j\to i} - \Delta t p_{i\to j} \\ &= -\Delta t \left(p_i(t) - \sum_{j=1}^{N} \frac{A_{ij}}{k_j} p_j(t) \right). \end{aligned} \tag{2.8}$$

The normalization condition can be checked by summing both sides over all nodes i. The left-hand side would instantly sum to zero, while the right-side eventually sums to zero because $\sum_{i=1}^{N} \frac{A_{ij}}{k_j} = 1$. This formulation captures the dynamics of the random walk, where the probability at each node evolves based on the probabilities at its neighboring nodes and the connectivity of the graph. As a result, the stationary distribution will be proportional to the degree of each vertex [9]. Rewriting Equation (2.8) in matrix form yields the differential equation:

$$\frac{d\mathbf{p}(\mathbf{t})}{dt} = -\mathfrak{L} D^{-1} \mathbf{p}(t) \equiv -H_C \mathbf{p}(t) \tag{2.9}$$

Where the Laplacian $\mathfrak{L}$ is chosen as in Equation (2.6). Furthermore, we have defined the classical Hamiltonian as we can compare it to the quantum case in Subsection 2.1.2. The solution to this equation with a certain initial distribution $\mathbf{p}(0)$ is given by

$$\mathbf{p}(t) = \mathbf{p}(0) e^{-H_C t} \tag{2.10}$$

For a finite connected graph $G = (V, E)$, the stationary distribution depends on both the degree of each vertex and the total number of edges in the graph. Intuitively, vertices with higher degrees tend to have higher probabilities of occupation for the walker.

In mathematical terms, for such graphs, the stationary distribution $\pi = (\pi_1, \pi_2, \ldots, \pi_n)$ is defined by:

$$\pi_i = \frac{k_i}{2|E|} \tag{2.11}$$

where k_i denotes the degree of vertex i (i.e., the number of edges incident to vertex i, and $|E|$ is the total number of edges in the graph G. Each π_i represents the probability of finding the walker at vertex i when the process reaches its stationary distribution. It can easily be shown that this is indeed the stationary distribution

To see that this is indeed the stationary distribution, note that the transition probability to go from node i to node j is given by $p_{i\to j} = \frac{1}{k_i}$ for $(i,j) \in E$. Therefore, the stationary distribution condition

$$\pi_j = \sum_i \pi_i p_{i\to j}$$

can be verified as follows:

$$\sum_i \pi_i p_{i\to j} = \sum_{(i,j)\in E} \frac{k_i}{2|E|}\frac{1}{k_i} = \sum_{(i,j)\in E} \frac{1}{2|E|} = \frac{k_j}{2|E|} = \pi_j.$$

The last two steps come from the fact that there are k_j edges adjacent to node j and we thus obtain the stationary distribution condition.

Let's now consider a line graph which is given by vertices $V = \{n_1, n_2, \ldots, n_N\}$ and edges $E = \{(n_i, n_{i+1}) \mid \forall i \in \{1, 2, \ldots, N-1\}\}$. For this finite graph ($|V| = N$), we can obtain a stationary distribution by calculating the transition matrix $P = D^{-1}A$ which corresponds to the term $\frac{A_{ij}}{k_j}$ in Equation 2.8 and solving for $\pi = \pi P$. The transitional matrix is then given by:

$$P = \begin{bmatrix} 0 & 1 & 0 & 0 & \cdots & 0 & 0 \\ \frac{1}{2} & 0 & \frac{1}{2} & 0 & \cdots & 0 & 0 \\ 0 & \frac{1}{2} & 0 & \frac{1}{2} & \cdots & 0 & 0 \\ 0 & 0 & \frac{1}{2} & 0 & \cdots & 0 & 0 \\ \vdots & \vdots & \vdots & \vdots & \ddots & \vdots & \vdots \\ 0 & 0 & 0 & 0 & \cdots & 0 & \frac{1}{2} \\ 0 & 0 & 0 & 0 & \cdots & 1 & 0 \end{bmatrix}. \tag{2.12}$$

The stationary distribution satisfies $\sum_{i=1}^{N} \pi_i = 1$, which yields the following result:

$$\pi = \begin{bmatrix} \frac{1}{2(N-1)} & \frac{1}{N-1} & \cdots \frac{1}{N-1} & \frac{1}{2(N-1)} \end{bmatrix} \tag{2.13}$$

2.3.2 Quantum random walks (QRW)

The quantum counterpart of the classical random walk we consider is continuous, meaning that it takes place entirely in a Hilbert space $\mathcal{H}$, contrasting with the discrete quantum random walk [1]. To establish this quantum analogue, we assign to each node i in the graph a basis vector represented in Dirac notation as $|i\rangle \in \mathcal{H}$. The Hilbert space $\mathcal{H}$ is a finite-dimensional complex vector space, specifically $\mathbb{C}^N$, for N nodes in the graph. These basis vectors are not only orthogonal but also normalized which is mathematically expressed as $\langle i|j\rangle = \delta_{ij}$. We pick our basis such that

$$|1\rangle = \begin{pmatrix} 1 \\ 0 \\ 0 \\ \vdots \\ 0 \end{pmatrix} \quad |2\rangle = \begin{pmatrix} 0 \\ 1 \\ 0 \\ \vdots \\ 0 \end{pmatrix} \quad \dots \quad |n\rangle = \begin{pmatrix} 0 \\ 0 \\ \vdots \\ 0 \\ 1 \end{pmatrix} \tag{2.14}$$

In this setup, the Hilbert space $\mathcal{H} = \mathbb{C}^N$ is spanned by the orthonormal basis vectors $\{|1\rangle, |2\rangle, \ldots, |n\rangle\}$, ensuring that any quantum state $|\Psi\rangle \in \mathcal{H}$ can be expressed as a linear combination of these basis states:

$$|\Psi\rangle = \sum_{i=1}^{n} \alpha_i |i\rangle,$$

for which $\alpha_i \in \mathbb{C}$ are complex coefficients satyisfying the normalization condition $\sum_{i=1}^{N} |\alpha_i|^2 = 1$.

The evolution of the random walk is described by the Lindbladian, which is discussed in Subsection 2.1.2.

The Hamiltonian that we use is the normalized graph Laplacian, given by:

$$H_Q = D^{-\frac{1}{2}} \mathfrak{L} D^{-\frac{1}{2}} \tag{2.15}$$

where D is the diagonal matrix of node degrees, and $\mathfrak{L}$ is the combinatorial Laplacian defined as $\mathfrak{L} = D - A$, with A being the adjacency matrix of the graph. This Hamiltonian, H_Q, is chosen specifically for several reasons:

- The normalized graph Laplacian H_Q ensures that the quantum walk is symmetric and unitary, preserving the probability distribution over the nodes. By normalizing with $D^{-\frac{1}{2}}$, the influence of node degree on the walk dynamics is balanced.

- The normalized graph Laplacian is similar to the classical Hamiltonian H_C in the sense that the evolution is determined by transition probabilities that are often proportional to node degrees. The quantum counterpart H_Q retains this property in a probabilistic sense.

- One of the key properties of H_Q is that the average long-time probability distribution for a system in the ground state of this Hamiltonian corresponds to the stationary distribution of the classical random walk. In classical walks, the stationary distribution is typically proportional to the node degrees, meaning that in the long run, the probability of finding the walker at a particular node is proportional to its degree. This property is mirrored in the quantum walk governed by H_Q, ensuring consistency between the classical and quantum descriptions.[10]

The significance of H_Q being symmetric lies in several aspects. Firstly, a symmetric matrix has real eigenvalues and orthogonal eigenvectors, which is crucial

for the stability of the quantum walk and for ensuring that the evolution operator $U(t) = e^{-iH_Q t}$ is well-behaved. Secondly, symmetry allows H_Q to be diagonalized by a unitary matrix Q, such that $H_Q = Q\Lambda Q^{-1}$, where Λ is the diagonal matrix of eigenvalues. This simplifies the computation of the matrix exponential used in the time-evolution operator. Lastly, symmetric Hamiltonians correspond to real, measurable physical observables in quantum mechanics, ensuring that the energy levels (eigenvalues) are real and that the evolution of the system is physically meaningful.

We can rewrite our unitary time-evolution operator $U(t) = e^{-iH_Q t}$ by diagonalizing the Hamiltonian, i.e. $H_Q = Q\Lambda Q^{-1}$ with eigenvalues λ_i and eigenvectors v_i. Using the definition of the matrix exponential, we obtain the following result:

$$\begin{aligned} e^{-iH_Q t} &= \sum_{m=0}^{\infty} \frac{(-it)^m}{m!} H_Q^m = \sum_{m=0}^{\infty} \frac{(-it)^m}{m!} (Q\Lambda Q^{-1})^m = \sum_{m=0}^{\infty} \frac{(-it)^m}{m!} Q\Lambda^m Q^{-1} \\ &= \sum_{m=0}^{\infty} \frac{(-it)^m}{m!} \sum_{i=1}^{N} \lambda_i^m \left|v_i\right\rangle \left\langle v_i\right| = \sum_{i=1}^{N} e^{-it\lambda_i} \left|v_i\right\rangle \left\langle v_i\right| \end{aligned} \tag{2.16}$$

This representation simplifies the analysis of the quantum walk, as it reduces the problem to the study of the eigenvalues and eigenvectors of H_Q.

Note that if we take our initial density matrix to be a superposition among all nodes, i.e. a normalized identity matrix $\rho(0) = \frac{1}{\sqrt{N}} I_N$, we can write equation 2.2 as follows:

$$\rho(t) = \frac{1}{\sqrt{N}} \sum_{i,j} e^{i(\lambda_i - \lambda_j)t} E_i E_j \tag{2.17}$$

for which we have defined $E_i = \left|v_i\right\rangle \left\langle v_i\right|$ and $E_j = \left|v_j\right\rangle \left\langle v_j\right|$. This equation shows that all elements of the density matrix will contain periodic terms with frequencies determined by the energies of the stationary states. An example will be shown in section 3.1 and 3.2.

2.4 Random walk search

A random walk search is a concept that can be studied in the classical and in the quantum domain. For the classical random walker, it usually takes random successive steps on a graph or lattice. At some point, it can reach a target state, or in other words, the state that you would like the walker to reach. These are called absorbing states such that the random walk is terminated when it reaches that specific state.

In many applications, one is interested in the expected time that it takes to reach this absorbing state, often referred to as the mean time to absorption (MTA). This is an important measure for the efficiency of search algorithms, diffusion models and other stochastic processes.

For the quantum random walk, it works rather differently. While it shares similarities with its classical counterpart, the evolution typically involves a superposition of states, which can lead to a faster search or absorption time if manipulated in a specific manner. In this section, we explore the concepts of random walk search for both the classical and quantum domain.

2.4.1 Classical random walk with absorbing target

As discussed, the classical random walk has been studied extensively regarding absorbing states or in the context of this thesis, target states. If you simulate a diffusion process without a reset rate, there is no guarantee that it reaches the absorption state. However, as it turns out the mean time to absorption (or reaching the target) is finite if you introduce a certain reset rate r [11].

For example, a well-known result from diffusion theory shows that a one-dimensional diffusion process with resetting rate r can be analyzed to obtain an expression for the mean time to absorption. In this process, the particle moves randomly along a line and is reset to a specific position X_r with rate r. The motion is governed by the diffusion constant D, which determines how quickly the parti-

cle moves or spreads out over time. The absorbing state in this case represents a boundary condition. Once the particle reaches this state, it is absorbed and reset to the reset state. This means that the absorbing state is not fixed, since you cannot predict where the particle will be when it resets. The expression for the mean time to absorption is given by:

$$\langle T(X_r)\rangle = \frac{1}{r}\left(e^{\alpha X_r} - 1\right). \tag{2.18}$$

Here, $\alpha = \sqrt{\frac{r}{D}}$ in which D is the diffusion constant. This has been plotted in Figure 2.1 where it clearly shows to have a minimum. This minimum, around $r = 2.54\,\mathrm{s}^{-1}$ is the optimal reset rate for reaching the target or absorbing state when using the reset position and diffusion constant are one.

Furthermore, Equation 2.18 shows that without resetting ($r = 0$), the search can take on an arbitrarily long time to reach the absorbing state.

As we will later see in Chapter 4, the quantum walk that we simulate there won't have an optimal reset rate, but depends on various other properties.

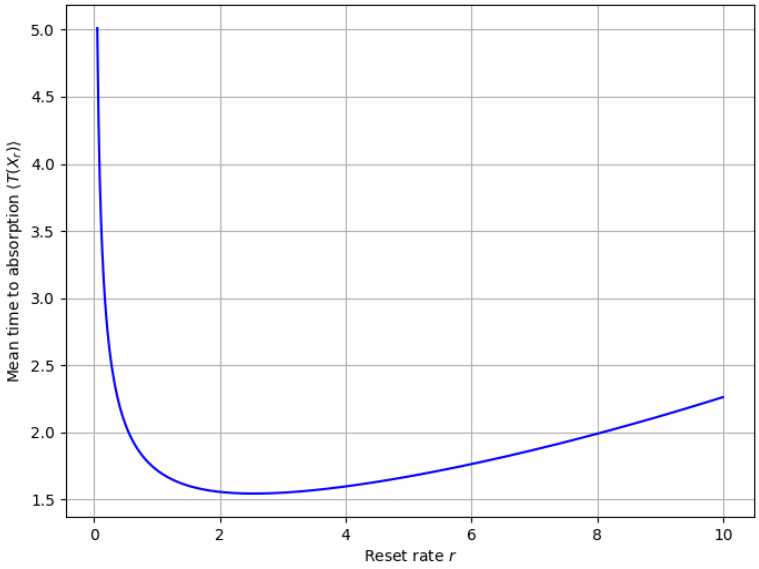

Figure 2.1 The mean time of absorption (MTA) plotted against the reset rate using Equation 2.18. The diffusion constant and the resetting position have been chosen to be one. Clearly, the reset rate has a minimum. The optimal reset rate in this case is approximately $r = 2.54\,\mathrm{s}^{-1}$.

2.4.2 Quantum random walk search

Quantum walks are frequently used to enhance the performance of classical algorithms. In this section we specifically look at how they are used to find a certain object or state in a network structure.

To have a higher probability of reaching that target state, we need the ground state of our Hamiltonian to be the target state. One way to achieve this, is by adding a term that lowers the energy for the target state and adding a factor that increases the energy of non-target states, as prescribed in [12]. This Hamiltonian is given below:

$$H_S = \gamma H_Q + H_w = \gamma D^{-\frac{1}{2}} \mathfrak{L} D^{-\frac{1}{2}} - \sum_w |w\rangle \langle w| \tag{2.19}$$

In our case we will only consider one target state, i.e. $-\sum_w |w\rangle \langle w| = -|w\rangle \langle w|$, but it is important to note that this framework can be used for multiple target states. An extra parameter would be needed in front of this term if $\gamma > 1$ to make

sure that the energy of the ground state is lowered and becomes the target state. This is due to the fact that H_Q is normalized using the degree matrix, but can be amplified by the γ in front of it. Considering the limits of this Hamiltonian, we have that when $\gamma \to \infty$, the ground state of the system will be described by H_Q and will be minimally influenced by the target Hamiltonian H_w. However, $\gamma = 0$ shows that the ground state is determined by the target Hamiltonian with H_S being a matrix with only one nonzero element. The eigenvectors of this matrix are given by $v_i = e_i$ and eigenvalues $\lambda_w = w$ and $\lambda_i = 0$ for $i \neq w$. This results in the constant $\rho(t) = \rho(0)$.

Example

Consider the Erdős–Rényi graph below and take as target state $|0\rangle$:

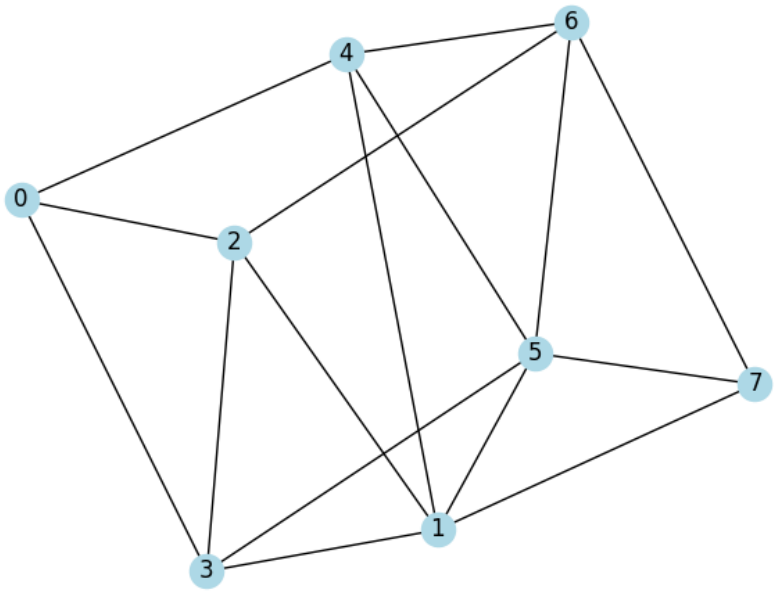

Figure 2.2 Erdős–Rényi graph $G_{8,\frac{1}{2}}$ consisting of eight nodes and each possible edge having $\frac{1}{2}$ probability of being included.

When simulating the search Hamiltonian H_S in equation 2.19, we can see what happens for multiple values of γ in figure 2.3. We can clearly see that for higher values of γ, the time-averaged probability (see equation 2.20) is lower and slowly converges to the distribution of the fully coherent quantum walk given by H_Q.

$$\langle p_i^{\gamma}(T)\rangle = \frac{1}{T}\int_0^T p_i(t)dt \quad \text{for } i \in \{0,1,\ldots,7\} \tag{2.20}$$

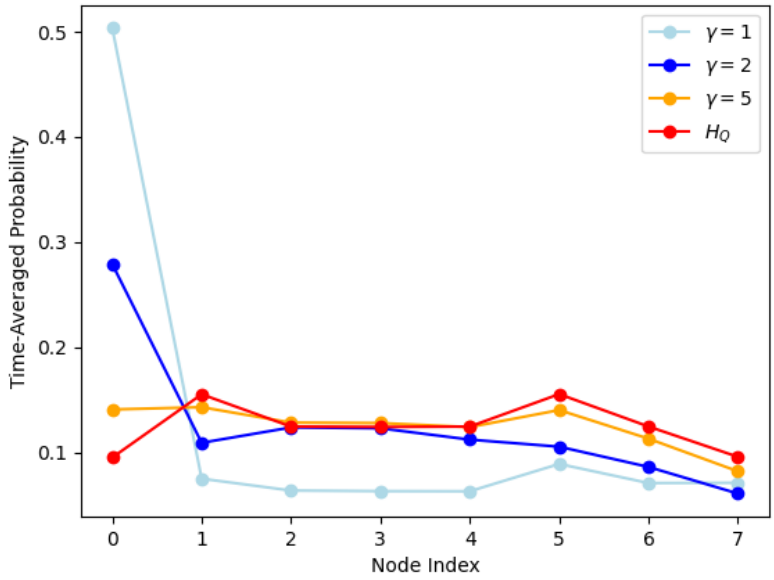

Figure 2.3 Time-averaged probability $\langle p_i^{\gamma}(T)\rangle$ plotted for all node indices $i \in \{0, 1, \ldots, 7\}$ in the Erdős–Rényi graph $G_{8,\frac{1}{2}}$ (see figure 2.2). In this simulation, $T = 200\,\mathrm{s}$, $dt = 0.01\,\mathrm{s}$, $\epsilon = 0$ (fully coherent) and the initial density matrix is a superposition over all states. The result has been checked for different values of T and remains unchanged. Note that for higher values of γ, the time averaged probability converges to the distribution prescribed by the quantum Hamiltonian H_Q, i.e. the nodes with the highest degree have highest time averaged probability.

This corresponds to our theoretical observation that the ground state is determined by the target state for lower values of γ. Furthermore we notice that the higher values of γ indeed converge to the fully coherent quantum walk given by H_Q. The initial condition, which in this case is a superposition over all states, is important since the evolution of the quantum walk starting from a pure state is slow and would impact the average excessively.

In Chapter 4, we try to optimize the probability of being in the target state by using resetting techniques.

2.4.3 Perturbation Theory

In this subsection, we apply perturbation theory to examine the effect of the search Hamiltonian H_S. The concept of perturbation theory is to treat the system as having two components. In this case, we have the base Hamiltonian $H_0 = \gamma H_Q$

which governs the evolution of the quantum walk and a perturbation V that influences the search for the target state.

The search Hamiltonian is therefore composed of the following components:

$$H_S = H_0 + V,$$

with

1. $H_0 = \gamma H_Q = \gamma D^{-\frac{1}{2}} \mathfrak{L} D^{-\frac{1}{2}}$ is the unperturbed Hamiltonian which corresponds to the quantum walk.

2. $V = -|w\rangle \langle w|$ is the perturbation term that lowers the energy of the target state $|w\rangle$, therefore leading the walker towards the target state.

We denote the eigenstate and eigenvalues of the unperturbed Hamiltonian H_0 as follows:

$$H_0 |\psi_n^{(0)}\rangle = E_n^{(0)} |\psi_n^{(0)}\rangle . \tag{2.21}$$

Here, $|\psi_n^{(0)}\rangle$ are the eigenstates and $E_n^{(0)}$ are the corresponding eigenvalues of H_0.

The first-order energy correction $E_n^{(1)}$ for the energy of the n-th state caused by the perturbation V is given by:

$$E_n^{(1)} = \langle \psi_n^{(0)}| V |\psi_n^{(0)}\rangle . \tag{2.22}$$

By using that $V = -|w\rangle \langle w|$, the correction term is dependent upon the overlap between the eigenstates $\psi_n^{(0)}$ and the target state $|w\rangle$. Therefore we have the following result:

$$E_n^{(1)} = -|\langle w|\psi_n^{(0)}\rangle|^2. \tag{2.23}$$

A worked out example can be found in Section 3.1.

A similar analysis can be done for the first-order wavefunction correction. This term is given by:

$$|\psi_n^{(1)}\rangle = \sum_{m \neq n} \frac{\langle \psi_m^{(0)}| V |\psi_n^{(0)}\rangle}{E_n^{(0)} - E_m^{(0)}} |\psi_m^{(0)}\rangle . \tag{2.24}$$

In our case, when substituting the perturbation term $V = -|w\rangle\langle w|$, we get the following expression:

$$|\psi_n^{(1)}\rangle = -\sum_{m\neq n} \frac{\langle\psi_m^{(0)}|w\rangle\langle w|\psi_n^{(0)}\rangle}{E_n^{(0)} - E_m^{(0)}} |\psi_m^{(0)}\rangle . \tag{2.25}$$

These corrections show how the target state influences the energy levels and wavefunctions of the system.

Chapter 3

Quantum Random Walk on Simple Graphs

In this chapter, we will be simulating the quantum random walk on simple graphs. We explore both the fully coherent and incoherent aspects of the walk, which are described respectively by the von Neumann equation and Lindblad master equation as discussed in subsection 2.1.2. Additionally, we will show some interesting properties that emerge from these simulations.

3.1 Path graph

A path graph shows interesting results when simulating both random walks discussed in section 2.3. This graph is constructed by numbering the nodes $V = \{n_1, n_2, \ldots, n_N\}$ and connecting the edges $E = \{(n_i, n_{i+1}) \mid \forall i \in \{1, 2, \ldots, N-1\}\}$. The result for the simulation is shown in Figure 3.1.

Note that for the quantum walk, two initial conditions were selected: the red line corresponds to a pure initial state on node n_{49}, while the orange line corresponds to a (normalized) superposition over all nodes. The latter is more spread out over the nodes and the walker has a higher probability of being observed on the outer nodes compared to the pure initial state. Additionally, the stationary distribution π for the classical walker has been plotted, as given by Equation 2.13.

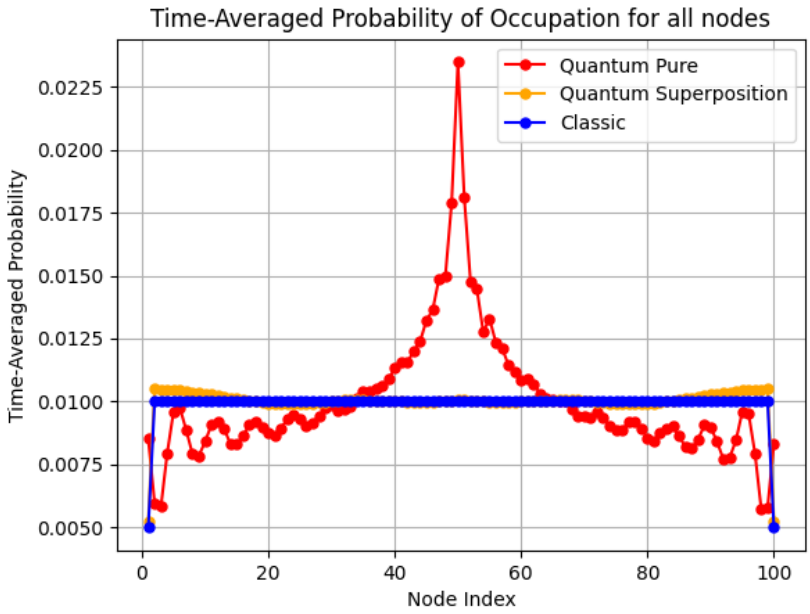

Figure 3.1 This graph shows the time-averaged probability of being at each node on a line graph consisting of $N = 100$ nodes for both a classical random walk (blue) and a quantum random walk (red and orange). For the quantum walk, two initial states were chosen: the red line corresponds to a pure state at node 50, and the orange line corresponds to a normalized superposition over all nodes. Both were simulated for 100 s according to the von-Neumann equation (see Equation 2.1). The time-averaged probability for the classical walk is the stationary distribution given in Equation 2.13. All walks exhibit symmetric behavior, which is expected given the symmetry of the graph. Over time, the quantum walk which started in the superposition tends to disperse more widely throughout the network compared to the classical walk and the pure state evolution, resulting in a greater likelihood of occupying nodes located further from the central region.

For relatively small graphs, it is possible to derive an analytical expression for the evolution of a quantum walk on a line graph. These analytical expressions are derived using the theory discussed in Section 2.3.

Let's consider a path graph containing $N = 5$ nodes. The graph Laplacian $\mathfrak{L} = D - A$ is given by:

$$\mathfrak{L} = \begin{bmatrix} 1 & -1 & 0 & 0 & 0 \\ -1 & 2 & -1 & 0 & 0 \\ 0 & -1 & 2 & -1 & 0 \\ 0 & 0 & -1 & 2 & -1 \\ 0 & 0 & 0 & -1 & 1 \end{bmatrix} \tag{3.1}$$

In this matrix, the entries on the diagonal come from the degree of each node, and the the other non-zero entries come from the adjacency matrix. Transforming this into the normalized graph Laplacian $H_Q = D^{-\frac{1}{2}}\mathfrak{L}D^{-\frac{1}{2}}$ yields:

$$H_Q = \begin{bmatrix} 1 & -\frac{1}{\sqrt{2}} & 0 & 0 & 0 \\ -\frac{1}{\sqrt{2}} & 1 & -\frac{1}{2} & 0 & 0 \\ 0 & -\frac{1}{2} & 1 & -\frac{1}{2} & 0 \\ 0 & 0 & -\frac{1}{2} & 1 & -\frac{1}{\sqrt{2}} \\ 0 & 0 & 0 & -\frac{1}{\sqrt{2}} & 1 \end{bmatrix} \tag{3.2}$$

We diagonalize this matrix such that we can later use it when calculating the unitary operator $U(t) = e^{-iH_Q t}$. The eigenvalues and eigenvectors of our Hamiltonian are given by:

$$\begin{aligned} \lambda_1 &= 0: & \mathbf{v}_1 &= \begin{bmatrix} 1 & \sqrt{2} & \sqrt{2} & \sqrt{2} & 1 \end{bmatrix}^{\mathrm{T}}, \\ \lambda_2 &= 1 - \frac{1}{2}\sqrt{2}: & \mathbf{v}_2 &= \begin{bmatrix} -1 & -1 & 0 & 1 & 1 \end{bmatrix}^{\mathrm{T}}, \\ \lambda_3 &= 1 + \frac{1}{2}\sqrt{2}: & \mathbf{v}_3 &= \begin{bmatrix} -1 & 1 & 0 & -1 & 1 \end{bmatrix}^{\mathrm{T}}, \\ \lambda_4 &= 1: & \mathbf{v}_4 &= \begin{bmatrix} 1 & 0 & -\sqrt{2} & 0 & 1 \end{bmatrix}^{\mathrm{T}}, \\ \lambda_5 &= 2: & \mathbf{v}_5 &= \begin{bmatrix} 1 & -\sqrt{2} & \sqrt{2} & -\sqrt{2} & 1 \end{bmatrix}^{\mathrm{T}} \end{aligned} \tag{3.3}$$

The eigenvalues correspond to the energy of the stationary states which are in turn described by the (normalized) eigenvectors. Our unitary operator now becomes:

$$U(t) = Q \begin{bmatrix} e^{-i\lambda_1 t} & 0 & 0 & 0 & 0 \\ 0 & e^{-i\lambda_2 t} & 0 & 0 & 0 \\ 0 & 0 & e^{-i\lambda_3 t} & 0 & 0 \\ 0 & 0 & 0 & e^{-i\lambda_4 t} & 0 \\ 0 & 0 & 0 & 0 & e^{-i\lambda_5 t} \end{bmatrix} Q^{-1} \tag{3.4}$$

Here, Q is the matrix whose columns are the eigenvectors of H_Q. Furthermore we have applied the exponent to the diagonal matrix containing the eigenvalues of H_Q.

For now we are only interested in the diagonal elements of the density matrix

$\rho(t) = U\rho(0)U^\dagger$, since they represent the pure states. We take the initial density matrix $\rho(0)$ as a 5×5-matrix with a single nonzero element in the center, representing the pure quantum state $|3\rangle$. More specifically, we have that $\rho_{33}(0) = 1$, such that we can express the diagonal entries of $\rho(t)$ as follows:

$$\rho_{ii}(t) = U_{i3}U_{i3}^* \quad \forall i \in \{1, 2, \ldots, 5\} \tag{3.5}$$

From this observation, we note that the elements of $\rho(t)$ are given by a linear combination of complex exponentials with a frequency that is determined by the energy or eigenvalues of the stationary states. Indeed, the (real) diagonal elements are given by (see Appendix A.1 for more details):

$$\begin{aligned}
\rho_{11}(t) = \rho_{55}(t) &= \frac{3}{16} - \frac{1}{8}\cos(\omega_{14}t) + \frac{1}{16}\cos(\omega_{15}t) - \frac{1}{8}\cos(\omega_{45}t) \\
\rho_{22}(t) = \rho_{44}(t) &= \frac{1}{8} - \frac{1}{8}\cos(\omega_{15}t) \\
\rho_{33}(t) &= \frac{3}{8} + \frac{1}{4}\cos(\omega_{14}t) + \frac{1}{8}\cos(\omega_{15}t) + \frac{1}{4}\cos(\omega_{45}t)
\end{aligned} \tag{3.6}$$

In which $\omega_{ij} \equiv \lambda_i - \lambda_j$ is the energy splitting between stationary states. Note that the average of each density matrix element $\bar{\rho}_{ii}(t)$ is given by the first term in Equation 3.6. This means that the average probability to be in the outer states $|1\rangle$ and $|5\rangle$ is higher than for states $|2\rangle$ and $|4\rangle$ as $\bar{\rho}_{11} = \frac{3}{16} > \frac{1}{8} = \bar{\rho}_{22}$. Both the simulated and theoretical result is shown in figure 3.2

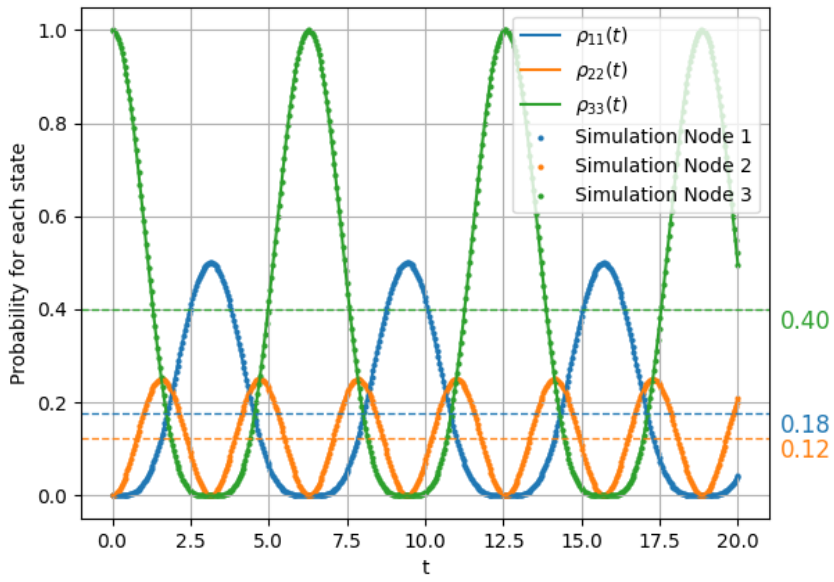

Figure 3.2 Theoretical probability of occupation for nodes one to three versus the numerically solved master equation in the `Qubit` Python package. The graph considered in this case is a line graph consisting of 5 nodes for which the time evolution is fully coherent, i.e. $\epsilon = 0$. Due to graph symmetry around node three, we have that $\rho_{11}(t) = \rho_{55}(t)$ and $\rho_{22}(t) = \rho_{44}(t)$. The averages are given by the first term in Equation 3.6.

We could however also use a different initial condition such as a superposition over all nodes/states. This can be represented by the density matrix with elements $\rho_{ij} = \frac{1}{5}$ for $i, j \in \{1, 2, \ldots, 5\}$. The result of this initial condition is shown in Figure 3.3. To derive this analytically, we can use Equation 2.2 and replace the previous pure state initial condition with the superposition of states initial condition. This yields the following result for the diagonal elements:

$$\rho_{ii}(t) = \frac{1}{5}\left[\left(\sum_{j=1}^{5} U_{ij}\right)\left(\sum_{k=1}^{5} U_{ik}^{*}\right)\right], \quad i \in \{1, 2, \ldots, 5\}. \tag{3.7}$$

Here, U_{ik}^{*} denotes the conjugate of matrix element U_{ik} which is the same matrix as in the pure state initial condition and can be seen in Appendix A.1.

An important difference is that the average probability for the center node $\bar{\rho}_{33}$ is subtantially lower when compared to the pure state initial condition seen in Figure 3.2. In other words, the average probabilities do not deviate as much

for all nodes and are closer to one another. So we conclude that starting in superpositions is a better way of looking for target states. This result is used in Section 4.1 to optimize that probability by occasionally resetting the state to a new superposition of states.

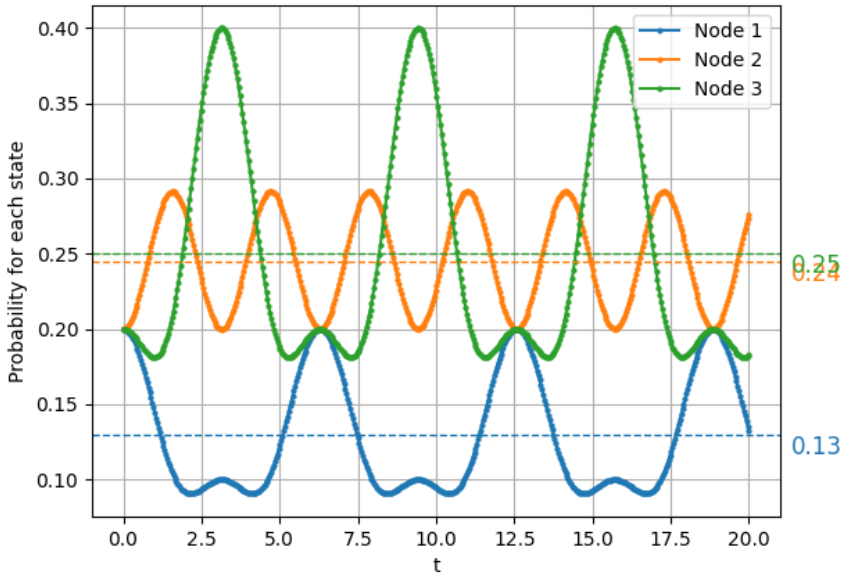

Figure 3.3 Simulation of a line graph consisting of $N = 5$ nodes using a superposition over all states as initial condition, i.e. $\rho_{ij}(0) = \frac{1}{5}$ for $i, j \in \{1, 2, \ldots, 5\}$. The average probability $\bar{\rho}_{ii}$ to be in a specific pure state is the same as the stationary distribution of a classical random walk on a graph, in contrast with the pure state initial condition.

Furthermore, if we allow for decoherences to take place, we observe that the probabilities start to decay exponentially to their respective classical probabilities, see Figure 3.4. In this figure, the probability for various values of ϵ is given by the diagonal element of the density matrix $\rho_{33}(t)$ of which the evolution is given by Equation 2.4. Multiple values of ϵ are shown in the figure to show how decoherence affects the probability to observe the quantum state $|3\rangle$.

Several key observations should be noted, including the damping of the oscillatory behavior when increasing ϵ. This effect is due to the jump operators that were added in the Lindblad equation. Eventually, the probability will exponentially drop to its classical value given by $\epsilon = 1$. However, the amplitude is not the only characteristic that is changing, as we also observe a slight frequency change

in which the frequency drops when increasing ϵ which is due to the damping of the jump operators.

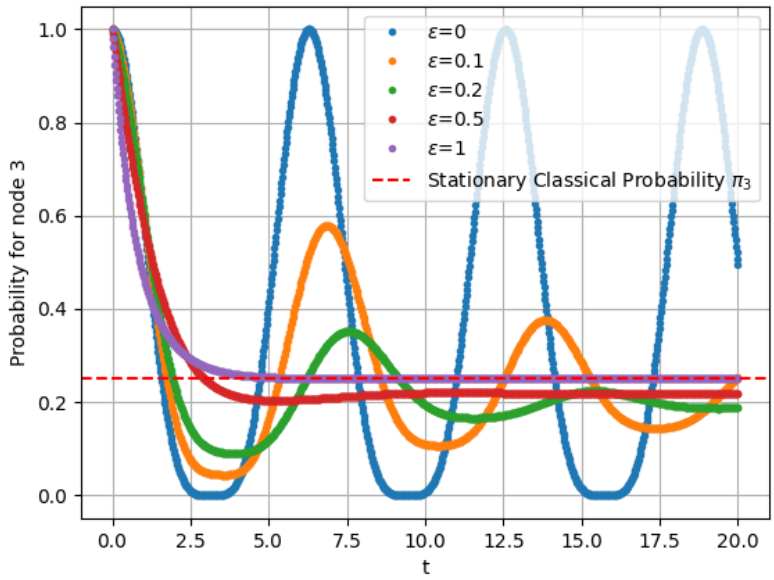

Figure 3.4 Diagonal density matrix element $\rho^{\epsilon}_{33}(t)$ for $\epsilon \in \{0, 0.1, 0.2, 0.5, 1\}$ plotted over time. Higher values of ϵ correspond to a stronger decoherence level where it eventually converges to the classical random walker stationary distribution probability π_3. This probability is described in section 2.3.1 and is given by $\pi_3 = \frac{k_3}{2|E|} = \frac{1}{4}$. A slight change in frequency is also noticeable with increasing ϵ, as the frequency clearly decreases. This is due to the damping phenomena of the jump operators.

If we now change our Hamiltonian to include the search term, as in Equation 2.19, we obtain the following equation for our system:

$$H_S = H_Q - |0\rangle \langle 0| \tag{3.8}$$

with $\gamma = 1$ and target state $|0\rangle$. Simulating this Hamiltonian with $\epsilon = 0$ gives interesting results as the probability to observe the quantum particle in the target state has increased a substantial amount, see Figure 3.5. This is what we expected as the ground state now corresponds to the target state, as discussed in Section 2.4. We observe strong oscillatory behaviour just as in Figure 3.2 since we have a fully coherent quantum state throughout time. This changes when we have a nonzero ϵ and implement decoherences into the simulation, as can be seen in Figure 3.6 where we have simulated the same configuration with $\epsilon = 0.1$. We can

see that after some period of time, the target state is not the most probable state to be observed and fades among the other states. In the next chapter, we will try to optimize this probability $\rho_{00}(t)$ by using resetting techniques.

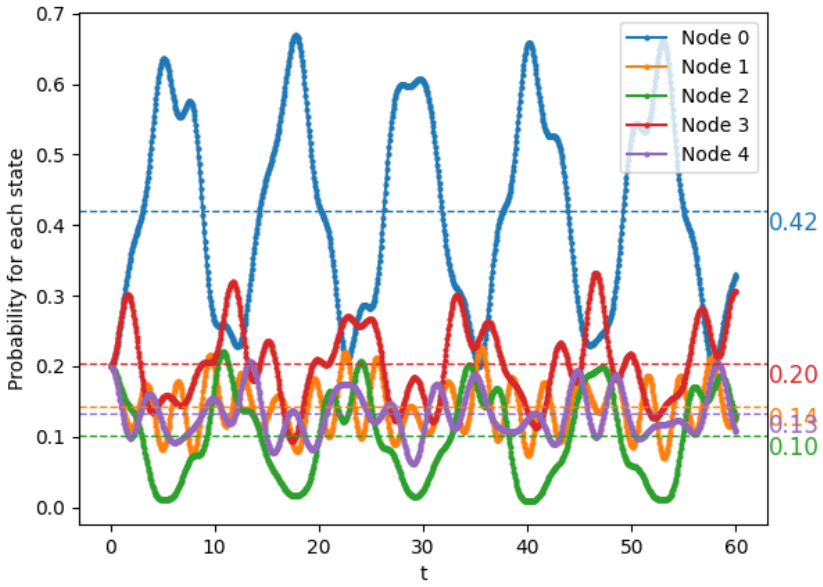

Figure 3.5 A simulation of a line graph consisting of $N = 5$ nodes with no decoherence ($\epsilon = 0$) in which the time evolution is characterised by the search Hamiltonian H_S in Equation 3.8. The averages are shown on the right side. For nodes zero to four, the probabilities are 0.42, 0.14, 0.10, 0.20, and 0.13, respectively.

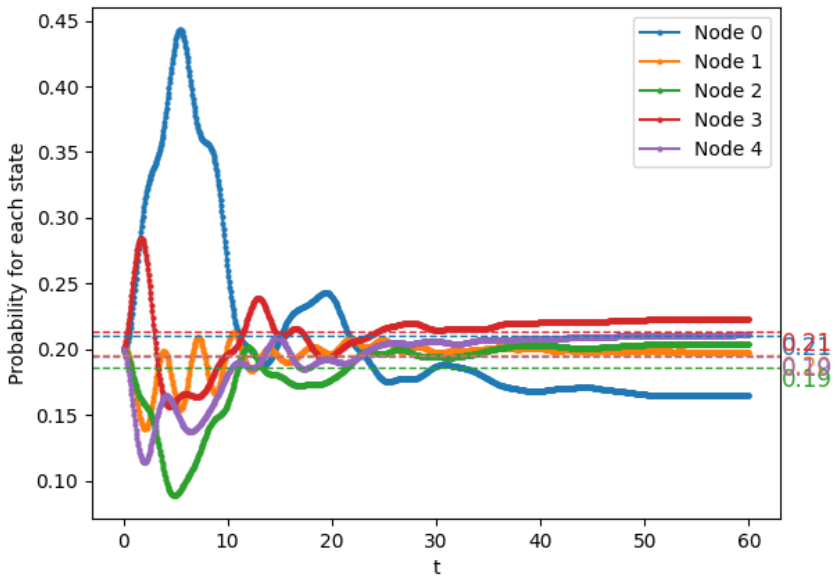

Figure 3.6 A simulation of a line graph consisting of $N = 5$ nodes with a slight decoherence level of $\epsilon = 0.1$. The time evolution is again described by the search Hamiltonian H_S in Equation 3.8. Note that we can only distinguish the target state within the first ten seconds of the simulation, after which it becomes equally probable to observe any other quantum state.

Further analysis can be done by using the perturbation theory as discussed in Section 2.4.3. For example, the first-order energy correction for the lowest energy state ψ_0 can be computed by normalizing the corresponding eigenvector in Equation 3.3. This results in:

$$E_0^{(1)} = -|\langle w|\psi_0\rangle|^2 = -\frac{1}{8} \tag{3.9}$$

As expected, the correction term turns out negative. The ground state energy is thus lowered and the probability of observing the walker in the ground state will be higher.

3.2 Cycle graph

Another interesting and analytically solvable graph is a cycle graph for which we can perform a similar analysis as compared to the line graph in section 3.1.

Let's consider a square graph ($N = 4$) for which the Laplacian is given by:

$$\mathfrak{L} = \begin{bmatrix} 2 & -1 & 0 & -1 \\ -1 & 2 & -1 & 0 \\ 0 & -1 & 2 & -1 \\ -1 & 0 & -1 & 2 \end{bmatrix} \tag{3.10}$$

Computing the Hamiltonian $H_Q = D^{-\frac{1}{2}}\mathfrak{L}D^{-\frac{1}{2}}$ (see Appendix A.2) and determining its eigenvalues and eigenvectors yields:

$$\begin{aligned} \lambda_1 = 0: &\qquad \mathbf{v}_1 = \begin{bmatrix} 1 & 1 & 1 & 1 \end{bmatrix}^{\mathrm{T}}, \\ \lambda_2 = 1: &\qquad \mathbf{v}_2 = \begin{bmatrix} -1 & 0 & 1 & 0 \end{bmatrix}^{\mathrm{T}}, \\ \lambda_3 = 1: &\qquad \mathbf{v}_3 = \begin{bmatrix} 0 & -1 & 0 & 1 \end{bmatrix}^{\mathrm{T}}, \\ \lambda_4 = 2: &\qquad \mathbf{v}_4 = \begin{bmatrix} -1 & 1 & -1 & 1 \end{bmatrix}^{\mathrm{T}} \end{aligned} \tag{3.11}$$

Again, using Q to denote the matrix constructed from the eigenvectors, we obtain an expression for $U(t)$:

$$U(t) = Q \begin{bmatrix} e^{-i\lambda_1 t} & 0 & 0 & 0 \\ 0 & e^{-i\lambda_2 t} & 0 & 0 \\ 0 & 0 & e^{-i\lambda_3 t} & 0 \\ 0 & 0 & 0 & e^{-i\lambda_4 t} \end{bmatrix} Q^{-1} \tag{3.12}$$

If we were to take $\rho(0)$ to be a superposition over all states, then that would coincide with the stationary distribution for the classical walk since all exponential terms would cancel out. Therefore, it is more interesting to look what happens to the evolution of a pure initial state $\rho(0) = |1\rangle\langle 1|$. Computing $\rho(t) = U\rho(0)U^\dagger$ yields the following expressions for the diagonal elements of the density matrix $\rho(t)$:

$$\begin{aligned} \rho_{11}(t) = \rho_{33}(t) &= \frac{3}{8} + \frac{1}{4}\cos(\omega_{12}t) + \frac{1}{8}\cos(\omega_{14}t) + \frac{1}{4}\cos(\omega_{24}t) \\ \rho_{22}(t) = \rho_{44}(t) &= \frac{1}{8} - \frac{1}{8}\cos(\omega_{14}t) \end{aligned} \tag{3.13}$$

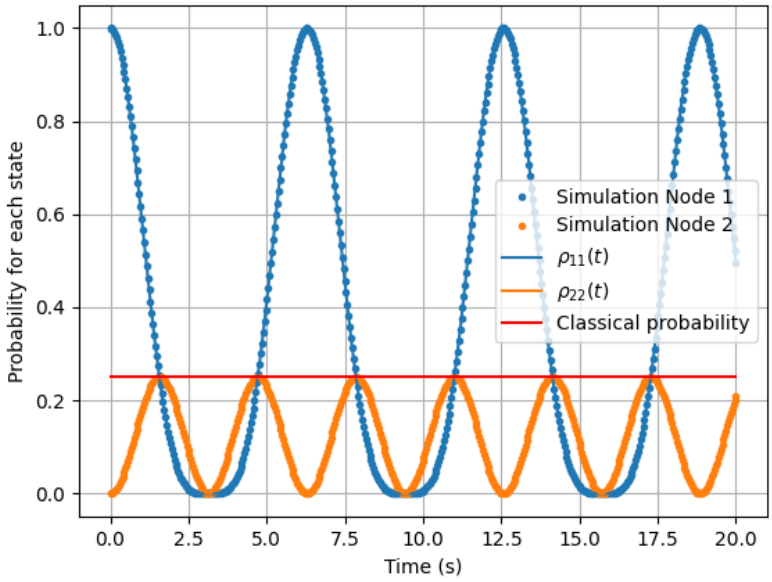

Figure 3.7 Theoretical probability of occupation for node one and two as well as the numerically solved master equation in the `Qubit` Python package. The red line is the stationary distribution for a classical walker, which coincides with the quantum evolution of a normalized superposition over all states.

If we now use the search Hamiltonian H_S to search for state/node $|1\rangle$, the Laplacian $\mathfrak{L}$ is changed to:

$$\mathfrak{L} = \begin{bmatrix} 1 & -1 & 0 & -1 \\ -1 & 2 & -1 & 0 \\ 0 & -1 & 2 & -1 \\ -1 & 0 & -1 & 2 \end{bmatrix} \tag{3.14}$$

Also, we take as initial state, a superposition over all states, since that has proven itself more useful when looking for a target state in Section 3.1. As we can see in Figure 3.8, the walker shows a much higher probability of being observed in target state $|1\rangle$. Another important observation is the fact that the probability of observation for adjacent nodes is lower than the opposite or further node, in this case $|3\rangle$.

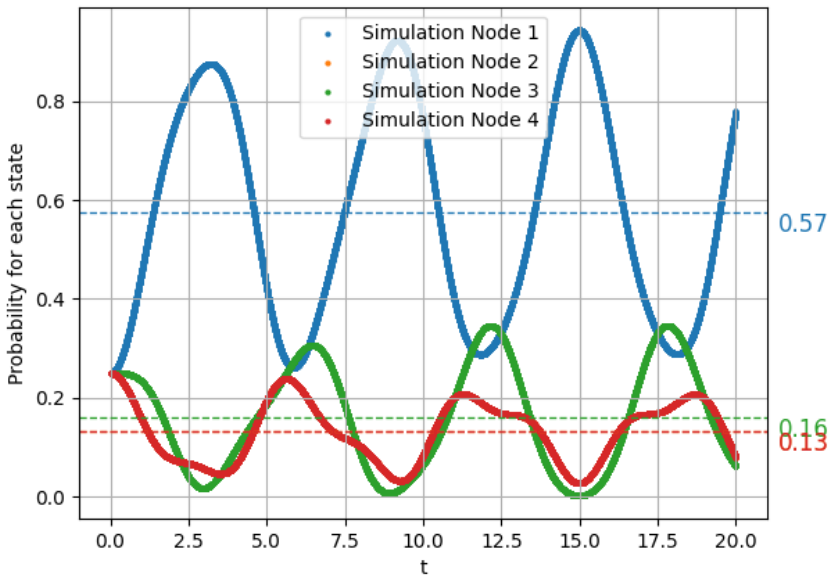

Figure 3.8 Probability for the walker to be in each state for a cycle graph containing $N = 4$ nodes and target state $|1\rangle$. Notice how the probability of being in state $|2\rangle$ and $|4\rangle$ is equal due to the symmetry of the graph. The probability of being in the opposite node or state, in this case $|3\rangle$ keeps slowly increasing. This is an important finding since it can be used for further optimization and faster convergence towards the target state.

Chapter 4

Resetting

Not only has it been shown that a quantum random walk can provide exponential speedup compared to a classical random walk [13], but also that it can be used for database searching [14]. This is due to the fact that a quantum random walk can be in a superposition of states and traverses the graph faster when compared to its classical counterpart, as discussed in section 3.1. In this chapter, we will show that resetting can help and optimize the process of finding a certain target node using the quantum walk search framework discussed in section 2.4. Furthermore, the reset process is needed to omit the effects of decoherence.

4.1 Constant resetting with dynamic reset state

First, we consider a scenario in which we reset the walker at a constant rate r and thus a reset time $\tau = \frac{1}{r}$, but change our reset state over time. Mathematically, this results in various stages of density matrix evolution denoted by $\rho(t)$. Note that if we were to maintain our reset state as constant, the system would not exhibit significant changes, as it would remain within the same evolutionary cycle. Therefore we consider two cases:

- The reset state is determined by the basis states that have the highest probability of being observed when resetting. Using the result of section 3.1, a superposition of states causes the evolution to be more scattered throughout the network in contrast with a pure state of which the average probability may peak in certain states. Therefore, we want to keep using superpositions

and choose this selection of highest probable states when resetting. For the next stage of density matrix evolution, we take a superposition of states containing the observed basis states, such that $\rho(t_i = \frac{i}{r}) = \frac{1}{|S_i|} \sum_{s_j, s_k \in S_i} |s_j\rangle \langle s_k|$, with $i \in \mathbb{N}$ and in which the set S_i contains the observed states at the i-th reset and the index i is the number of resets. Here, we assume that we fully know the probability distribution of observing each state at times $t_i = \frac{i}{r}$ with $i \in \{0, 1, \ldots, R\}$, else we cannot know the states with the highest probability of being observed. Practically, one would thus have to measure multiple times to get an idea of the state distribution. Furthermore, we have that $|S_i| = |S_j|$ for $i, j \in \{0, 1, \ldots, R\}$, such that the number of bases is fixed.

- The reset state is again a superposition of states but instead of a fixed number of bases in the superposition, it decreases throughout time, such that the reset algorithmically converges to the pure target state.

These cases are motivated by the problem of maximizing the probability of observing the target state in the shortest amount of time. The evolution will be described by the Lindblad master equation, as expressed in equation 2.4, which includes the parameter ϵ to simulate and amplify either the coherent or incoherent component.

Various simulations are shown in Figure 4.1. The graph for these simulations is an Erdős–Rényi graph with $N = 10$ and $p = 0.5$ such that each possible edge is chosen with probability p. The target state has been set on state or node $|4\rangle$ and multiple scenarios have been simulated for $|S_i| \in \{3, 5\}$ and reset rate $r \in \{0.1, 0.3\}$. The figure illustrates that you want to keep $|S_i|$ small since the probability for $|S_i| = 3$ is eventually higher for the target state when compared to the other scenarios. However, at the beginning of the evolution, a smaller $|S_i|$ is more advantageous. This can be seen by the fact that the target state $|4\rangle$ reaches a higher probability early on.

On top of that, the optimization of the reset rate r is also not straightforward. This can be seen in scenario three and four, where the higher reset rate $r = 0.3$ eventually has the best average probability for the target state but only after three

resets. The smaller reset rate $r = 0.1$ reaches a higher probability much quicker and needs only one reset before entering a series of cycles.

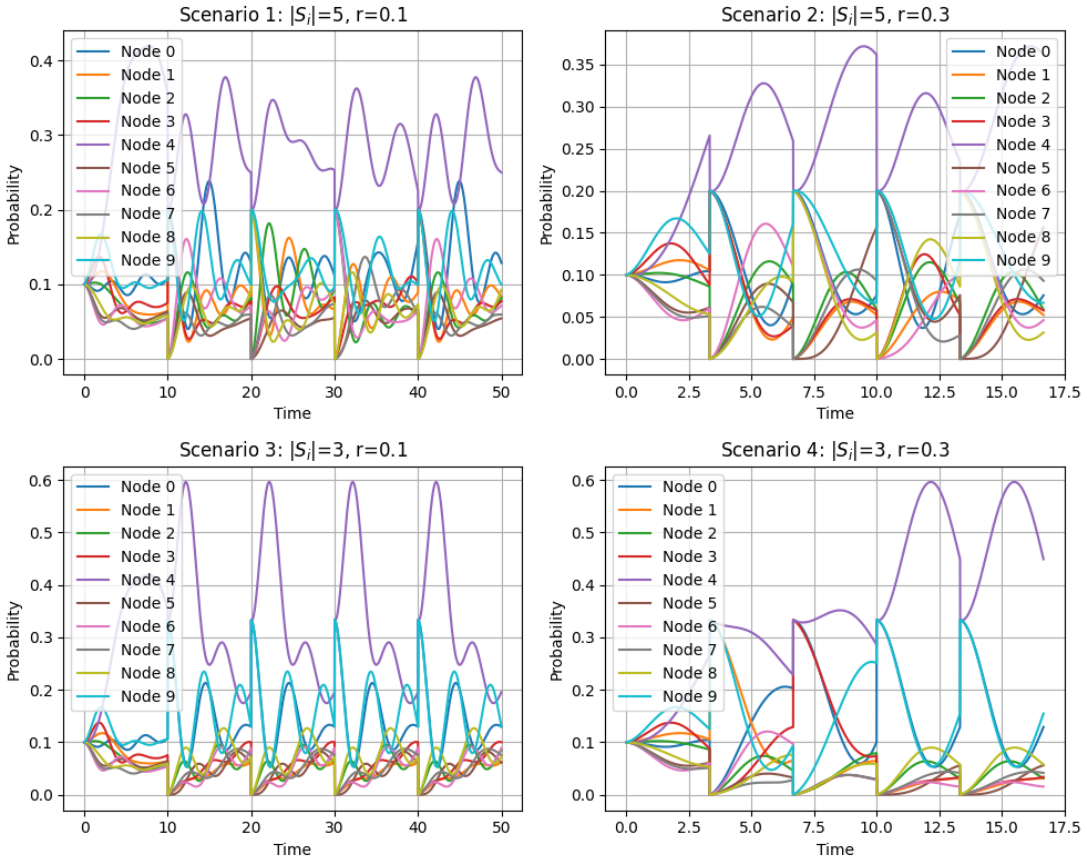

Figure 4.1 Erdős–Rényi graph $G_{10,\frac{1}{2}}$ consisting of $N = 10$ nodes and a probability of $p = \frac{1}{2}$ for each edge to be included. The reset rate r is varied with $r \in \{0.3, 0.5\}$, the dimensionality of the reset state is varied as well with $|S_i| \in \{3, 5\}$. Furthermore, the decoherence level has been set at $\epsilon = 0.1$. As can be seen when comparing scenario one and three, it is more advantageous to have a lower dimensionality for the reset state. However, this comes at a cost because it converges slower to the target state $|4\rangle$ when looking at scenario two and four. The reset rate should also be between a certain margin, as for higher values of r, the evolution converges slower to the target state. In contrast, the lower values of r lead to lower probabilites throughout the evolution.

4.2 Constant resetting to dynamic superposition dimensionality

As described in previous Section 4.1, we can change the dimensionality of the reset state $|S_i|$ over time. This will help to let the walker converge to the target state with complete assurance since $|S_i| \to 1$ as $t \to \infty$. An exponential function can

best be used to obtain this convergence property and to quickly reach the target state. For example, consider the exponential decay function of the form:

$$f(x) = 1 + (a - 1)e^{-bx} \tag{4.1}$$

where $a, b \in \mathbb{R}$ with $a > 1$ and $b > 0$. This would make sure that the walker quickly converges to the target state due the exponential decay, starting from superposition dimensionality a. Not only that, the reset state would be the pure target state eventually as the superposition dimensionality converges to one.

An example of this is shown in Figure 4.2 where we used Equation 4.1 to let the dimensionality of the reset state converge to one. This is the optimal result for this specific graph as it enters a loop after reset $i = 8$ in which the probability of observing the target state $|4\rangle$ is almost one. Further optimization would be possible if we were to increase the reset rate linearly or exponentially with each reset.

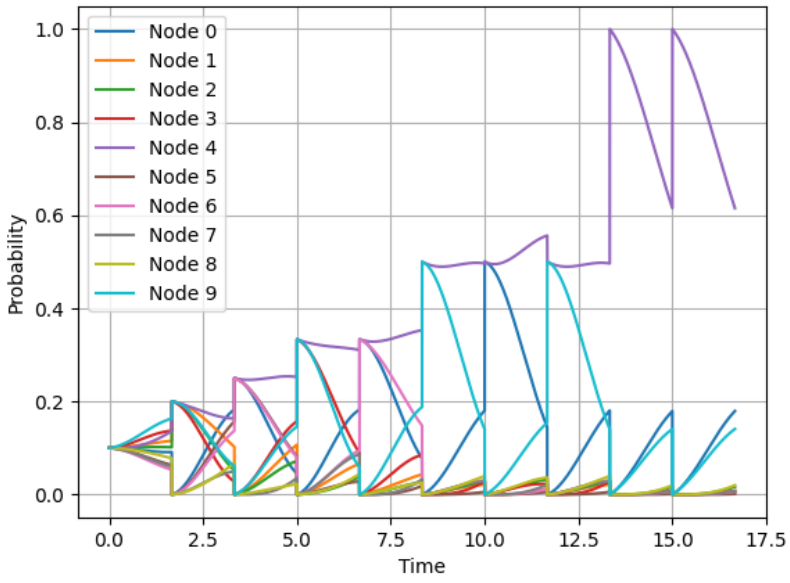

Figure 4.2 Erdős–Rényi graph $G_{10,\frac{1}{2}}$ consisting of $N = 10$ nodes and a probability of $p = \frac{1}{2}$ for each edge to be included. The decoherence level is $\epsilon = 0.1$ and the dimensionality of the reset state is described by Equation 4.1 with the parameters $a = 5$ and $b = 0.2$. The number of resets is $R = 9$ and the target state is $|4\rangle$.

Chapter 5

Conclusions

This thesis has explored the optimization of quantum random walk search algorithms using resetting techniques. The goal was to have a faster convergence towards a pure target state together while dealing with decoherence effects that take place in an open quantum system.

We began by discussing the theoretical framework that was needed, including important principles and concepts from quantum mechanics, focusing on the Lindblad master equation for open systems. This equation provides the basis for modelling quantum random walks in open systems where interactions with the environment are accounted for. The normalized graph Laplacian was used as the Hamiltonian that controls the evolution of the quantum walk. We were able to simulate the quantum interactions on various graphs using the `QuTip` Python library.

Our simulations demonstrated the effect of a modified Hamiltonian, which was backed up using perturbation theory. The simulations provided concrete examples for simple graphs like path and cycle graphs. These graphs were also analytically studied which provided a broader understanding of the quantum walk.

The importance of this thesis lies in the application of resetting techniques to quantum random walks. We discussed two important strategies: constant resetting to a fixed dimensionality reset state that changes throughout time and resetting to a variable dimensionality reset state. Our findings show that resetting

towards a variable dimensionality super position optimizes the probability of finding the target state, while at the same time mitigating the effects of decoherence. In this process, we did make the assumption that you know the full probability space of the evolution when resetting. Although this is clearly not true, by performing the evolution a few times, it can still be practically applicable. On top of this, large graphs could not be analyzed using simulations because of computational difficulties. This makes it such that the limit of the resetting techniques is still unknown regarding larger graphs.

In conclusion, this thesis contributes to the understanding of quantum random walk search algorithms and how they can be optimized using resetting techniques. We provided frameworks and concepts for more efficient quantum searches which still have to be explored on more complex networks and real-world quantum systems. This creates an opening for possible future work, that could focus on testing the limit of our resetting techniques.

References

[1] J. Kempe, "Quantum random walks: An introductory overview", *Contemporary Physics*, vol. 44, no. 4, pp. 307–327, 2003.

[2] D. J. Griffiths and D. F. Schroeter, *Introduction to quantum mechanics*, Third edition. Cambridge ; New York, NY: Cambridge University Press, 2018.

[3] H.-P. Breuer and F. Petruccione, *The Theory of Open Quantum Systems*. Oxford University Press, January 2007.

[4] S. Wald and L. Böttcher, "From classical to quantum walks with stochastic resetting on networks", *Phys. Rev. E*, vol. 103, p. 012 122, 1 January 2021.

[5] F. Chung and W. Zhao, "Pagerank and random walks on graphs", in *Fete of Combinatorics and Computer Science*, G. O. H. Katona, A. Schrijver, T. Szőnyi, and G. Sági, Eds. Berlin, Heidelberg: Springer Berlin Heidelberg, 2010, pp. 43–62.

[6] C. Gkantsidis, M. Mihail, and A. Saberi, "Hybrid search schemes for unstructured peer-to-peer networks", vol. 3, 1526–1537 vol. 3, 2005.

[7] E. F. Fama, "Random walks in stock market prices", *Financial Analysts Journal*, vol. 21, pp. 55–59, 1965.

[8] N. Shenvi, J. Kempe, and K. B. Whaley, "Quantum random-walk search algorithm", *Physical Review A*, vol. 67, p. 052 307, 2002.

[9] G. Grimmett and D. Welsh, *Probability: An Introduction*. Oxford University Press, 2014.

[10] M. Faccin, T. Johnson, J. Biamonte, S. Kais, and P. Migdał, "Degree distribution in quantum walks on complex networks", *Phys. Rev. X*, vol. 3, p. 041 007, 4 October 2013.

[11] M. R. Evans, S. N. Majumdar, and G. Schehr, "Stochastic resetting and applications", *Journal of Physics A: Mathematical and Theoretical*, vol. 53, no. 19, p. 193 001, April 2020.

[12] A. M. Childs and J. Goldstone, "Spatial search by quantum walk", *Phys. Rev. A*, vol. 70, p. 022 314, 2 August 2004.

[13] A. M. Childs, R. Cleve, E. Deotto, E. Farhi, S. Gutmann, and D. A. Spielman, "Exponential algorithmic speedup by a quantum walk", STOC03, 2003.

[14] L. K. Grover, "A fast quantum mechanical algorithm for database search", 1996.

Appendix A

A.1 Line graph

$$U = \begin{bmatrix} 1 & -1 & -1 & 1 & 1 \\ \sqrt{2} & -1 & 1 & 0 & -\sqrt{2} \\ \sqrt{2} & 0 & 0 & -\sqrt{2} & \sqrt{2} \\ \sqrt{2} & 1 & -1 & 0 & -\sqrt{2} \\ 1 & 1 & 1 & 1 & 1 \end{bmatrix} \begin{bmatrix} e^{-i\lambda_1 t} & 0 & 0 & 0 & 0 \\ 0 & e^{-i\lambda_2 t} & 0 & 0 & 0 \\ 0 & 0 & e^{-i\lambda_3 t} & 0 & 0 \\ 0 & 0 & 0 & e^{-i\lambda_4 t} & 0 \\ 0 & 0 & 0 & 0 & e^{-i\lambda_5 t} \end{bmatrix} \begin{bmatrix} \frac{1}{8} & \frac{\sqrt{2}}{8} & \frac{\sqrt{2}}{8} & \frac{\sqrt{2}}{8} & \frac{1}{8} \\ -\frac{1}{4} & -\frac{1}{4} & 0 & \frac{1}{4} & \frac{1}{4} \\ -\frac{1}{4} & -\frac{1}{4} & 0 & -\frac{1}{4} & \frac{1}{4} \\ \frac{1}{4} & 0 & -\frac{\sqrt{2}}{4} & 0 & \frac{1}{4} \\ \frac{1}{8} & -\frac{\sqrt{2}}{8} & \frac{\sqrt{2}}{8} & -\frac{\sqrt{2}}{8} & \frac{1}{8} \end{bmatrix}$$

Diagonal Density Matrix Element for a Pure State Initial Condition:

General form:

$$\rho_{ii}(t) = U_{i3}U_{i3}^*, \quad i \in \{1, 2, \ldots, 5\}$$

First diagonal element $\rho_{11}(t)$:

$$\begin{aligned} \rho_{11}(t) = U_{13}U_{13}^* &= \left(\frac{\sqrt{2}}{8}e^{-i\lambda_1 t} - \frac{\sqrt{2}}{4}e^{-i\lambda_4 t} + \frac{\sqrt{2}}{8}e^{-i\lambda_5 t}\right)\left(\frac{\sqrt{2}}{8}e^{i\lambda_1 t} - \frac{\sqrt{2}}{4}e^{i\lambda_4 t} + \frac{\sqrt{2}}{8}e^{i\lambda_5 t}\right) \\ &= \frac{3}{16} - \frac{1}{8}\cos(\omega_{14}t) + \frac{1}{16}\cos(\omega_{15}t) - \frac{1}{8}\cos(\omega_{45}t) \end{aligned}$$

Diagonal Density Matrix Element for a Superposition of States Initial Condition:

$$\rho_{ii}(t) = \frac{1}{5}\left[\left(\sum_{j=1}^{5} U_{ij}\right)\left(\sum_{k=1}^{5} U_{ik}^*\right)\right], \quad i \in \{1, 2, \ldots, 5\}.$$

A.2 Cycle graph

$$H_Q = D^{-\frac{1}{2}}\mathcal{L}D^{-\frac{1}{2}} = \begin{bmatrix} 1 & -\frac{1}{2} & 0 & -\frac{1}{2} \\ -\frac{1}{2} & 1 & -\frac{1}{2} & 0 \\ 0 & -\frac{1}{2} & 1 & -\frac{1}{2} \\ -\frac{1}{2} & 0 & -\frac{1}{2} & 1 \end{bmatrix}$$

$$U(t) = \begin{bmatrix} 1 & -1 & 0 & -1 \\ 1 & 0 & -1 & 1 \\ 1 & 1 & 0 & -1 \\ 1 & 0 & 1 & 1 \end{bmatrix} \begin{bmatrix} e^{-i\lambda_1 t} & 0 & 0 & 0 \\ 0 & e^{-i\lambda_2 t} & 0 & 0 \\ 0 & 0 & e^{-i\lambda_3 t} & 0 \\ 0 & 0 & 0 & e^{-i\lambda_4 t} \end{bmatrix} \begin{bmatrix} \frac{1}{4} & \frac{1}{4} & \frac{1}{4} & \frac{1}{4} \\ -\frac{1}{2} & 0 & \frac{1}{2} & 0 \\ 0 & -\frac{1}{2} & 0 & \frac{1}{2} \\ -\frac{1}{4} & \frac{1}{4} & -\frac{1}{4} & \frac{1}{4} \end{bmatrix}$$

$$\begin{aligned} \rho_{11}(t) = U_{11}U_{11}^* &= \left(\frac{1}{4}e^{-i\lambda_1 t} + \frac{1}{2}e^{-i\lambda_2 t} + \frac{1}{4}e^{-i\lambda_4 t}\right)\left(\frac{1}{4}e^{i\lambda_1 t} + \frac{1}{2}e^{i\lambda_2 t} + \frac{1}{4}e^{i\lambda_4 t}\right) \\ &= \frac{3}{8} + \frac{1}{4}\cos\left(\omega_{12}t\right) + \frac{1}{8}\cos\left(\omega_{14}t\right) + \frac{1}{4}\cos\left(\omega_{24}t\right) \end{aligned}$$

A.3 Code

The Python code that was used to simulate various quantum walks and create the figures can be found on Github using this link: https://github.com/Mystery4U/quantum_walk